Computers and Electronics in Agriculture 124 (2016) 23–28

Contents lists available at ScienceDirect

Computers and Electronics in Agriculture

journal homepage: www.elsevier.com/locate/compag

Stress wave velocity patterns in the longitudinal–radial plane of trees for defect diagnosis

Guanghui Li [a,b,*], Xiang Weng [c], Xiaocheng Du [c], Xiping Wang [d], Hailin Feng [c]

[a] School of Internet of Things (IoT) Engineering, Jiangnan University, Wuxi, China
[b] Engineering Research Center of IoT Technology Applications (Ministry of Education), Jiangnan University, Wuxi, China
[c] School of Information Engineering, Zhejiang A&F University, Hangzhou, China
[d] USDA Forest Service, Forest Products Laboratory, Madison, WI, USA

A R T I C L E I N F O

Article history:
Received 29 October 2015
Received in revised form 22 March 2016
Accepted 25 March 2016

Keywords:
Defect
Inspection
Nondestructive testing
Stress wave velocity
Urban trees

A B S T R A C T

Acoustic tomography for urban tree inspection typically uses stress wave data to reconstruct tomographic images for the trunk cross section using interpolation algorithm. This traditional technique does not take into account the stress wave velocity patterns along tree height. In this study, we proposed an analytical model for the wave velocity in the longitudinal–radial (*LR*) plane of a live tree. Both field and laboratory stress wave testing were conducted to determine the stress wave velocity patterns in healthy and defective trees. The results showed that the ratio of the wave velocity at a propagation path angle θ (with respect to the radial direction) to the radial velocity in healthy trees approximated a second-order parabolic curve with respect to the symmetric axis ($\theta = 0$). Our analysis of the velocity patterns indicated that the measured velocities in healthy trees were in a good agreement with the theoretical models. The results of this preliminary study indicated that the stress wave velocity patterns can be used to diagnosis internal defects in urban trees and improve the accuracy of 3D tomographic images in tree inspection applications.

1. Introduction

Effective nondestructive testing methods capable of locating and quantifying wood decay and defects are needed by urban forest managers and arborists to determine the physical condition of trees and promote public safety. As a simple and low-cost nondestructive testing technique, stress wave method has been commonly used to assess internal conditions of wood structural members in buildings, timber bridges, and other timber structures (Pellerin and Ross, 2002; Ross and Pellerin, 1994). Stress wave velocity measured in trees has also been found effective in detecting moderate to severe decay in urban trees (Lawday and Hodeges, 2000; Wang et al., 2004; Wang, 2013; Hasegawa et al., 2012; Najafi et al., 2009; Guntekin et al., 2013). More recent development of efficient inversion algorithms enables stress wave techniques to be applied to urban trees to construct two dimensional (2D) acoustic tomograms for better revealing the internal condition of a tree trunk (Berndt et al., 1999; Bucur, 2003; Divos and Divos, 2005; Lin et al., 2008; Socco et al., 2004). Some commercial acoustic equipment such as Picus Sonic Tomograph (Argus Electronic Gmbh, Rostock, Germany), ArborSonic 3D Acoustic Tomograph (Fakopp Enterprise, Agfalva, Hungary), and Arbotom (RinnTech, Heidelberg, Germany) are now available for inspectors to obtain a 2D tomogram image by testing a tree's cross-section or 3D tomogram images through testing multiple cross-sections in a tree trunk.

However, the interpretation of an acoustic tomogram is not straight forward. A better understanding of wave velocity patterns in trees is critical to developing reliable and effective imaging software for internal decay detection. Dikrallah et al. (2006) presented an experimental analysis of acoustic anisotropy of wood, in particular the dependence of propagation velocities of stress waves on natural anisotropy axis in the cross section. They reported a significant difference in wave velocity between the waves propagating through the whole volume and the waves guided on bars. Maurer et al. (2005) studied the anisotropy effects on time-of-flight based tomography assuming an elliptic anisotropy where the angle dependent velocity v can be written as $v = v_{radial}\,(1 - \varepsilon\sin(\phi - \varphi)^2)$, where ϕ is the ray angle, φ represents the azimuth of the v_{radial} direction relative to the axis of the coordinate system, and ε specifies the degree of anisotropy. Liang et al. (2010) showed that stress waves traveled fastest in radial direction and that velocity decreased as the wave propagation path

* Corresponding author at: School of Internet of Things (IoT) Engineering, Jiangnan University, Wuxi, China.

E-mail address: ghli@jiangnan.edu.cn (G. Li).

http://dx.doi.org/10.1016/j.compag.2016.03.021
0168-1699/

shifted toward to tangential direction. Velocity also increased as the number of annual rings increased. Li et al. (2014) studied stress wave velocity patterns in black cherry trees and found that the ratio of tangential velocity to radial velocity in sound healthy trees approximated a second-order parabolic curve with respect to the symmetric axis $\theta = 0$ (θ is the angle between wave propagation path and radial direction). The analytical model was found in excellent agreement with the real data from healthy trees. Socco et al. (2004) also pointed out that the marked anisotropy of longitudinal direction properties could create numerous difficulties in constructing 3D tomographic images for trees. They considered longitudinal velocity a "less diagnostic" parameter for decay detection than the corresponding tangential and radial velocity. In investigating the effect of grain angle on longitudinal stress wave velocity in lumber, Gerhards (1982) found that grain angle had a greater effect on speed: over 1 percent loss per degree increase in grain angle up to about 30°. The effect of grain angle on MOE and tensile strength can be approximated by the Hankinson-type formula (USDA Forest Products Laboratory, 2010).

The objectives of this study were to investigate the stress wave velocity patterns in the *LR* plane of live trees and examine the effect of internal tree defect on the velocity pattern. We proposed a theoretical model of longitudinal wave velocity in *LR* plane of sound live trees and demonstrated the effectiveness of the theoretical model as a tool for tree defect diagnosis.

2. Theoretical analysis of stress wave velocity pattern in *LR* plane of live trees

Fig. 1 shows the coordinate system of an ideal tree trunk. Here, *L* represents the longitudinal or fiber direction, *R* represents the radial direction, and *T* is the tangential direction. For a longitudinal stress wave testing of wood, assume that ***OS*** is the stress wave propagation path in the *LR* plane, ***O*** is the first sensor for collecting the start stress wave signal, and ***S*** is the second sensor for sensing the propagating wave signal. In addition, α is the angle between the wave propagation path and the fiber direction, and θ is the angle between radial direction and the wave propagation path. So, $\alpha + \theta = 90°$.

Hankinson's formula provides a mathematical relationship that can be used to predict the off-axis uniaxial compressive strength of wood. The formula can also be used to compute the fiber stress or the stress wave velocity as a function of grain angle in wood (Li et al., 2014). The stress wave velocity at grain angle α can be obtained from the Hankinson formula:

$$V(\alpha) = \frac{V_l V_r}{V_l \sin^2\alpha + V_r \cos^2\alpha} \quad (1)$$

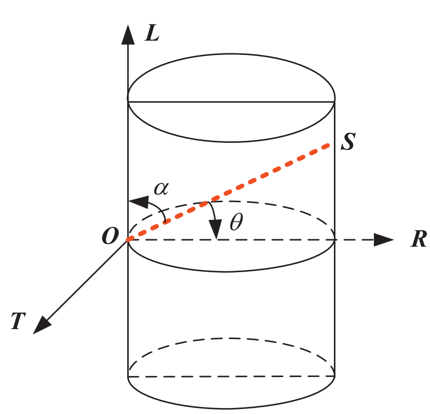

Fig. 1. The coordinate system of the tree trunk.

where V_l is the velocity parallel to the grain, V_r is the velocity perpendicular to the grain (or the velocity along the radial direction), which can be measured by the stress wave testing equipment.

Because $\alpha + \theta = 90°$, formula (1) can be converted into the following forms:

$$V(\theta) = \frac{V_l V_r}{V_l \cos^2\theta + V_r \sin^2\theta} \quad (2)$$

or

$$V(\theta)/V_r = \frac{V_l}{V_l \cos^2\theta + V_r \sin^2\theta} \quad (3)$$

Let $f(\theta) = V(\theta)/V_r$, and $g(\theta) = V_l \cos^2\theta + V_r \sin^2\theta$. From Eq. (3), it can be seen that, if $\theta = 90°$, then $f(\theta) = V_l/V_r$, and that if $\theta = 0°$, then $f(\theta) = 1$.

Now, we approximate Eq. (3) with the second order Taylor polynomial.

The first and second order derivatives of $f(\theta)$ and $g(\theta)$ are calculated as follows.

$$g'(\theta) = -2V_l \cos\theta \sin\theta + 2V_r \sin\theta \cos\theta = -(V_l - V_r)\sin 2\theta \quad (4)$$

$$g''(\theta) = -2(V_l - V_r)\cos 2\theta \quad (5)$$

$$f'(\theta) = -V_l (g(\theta))^{-2} g'(\theta) \quad (6)$$

$$f''(\theta) = -V_l\left(-2(g(\theta))^{-3}(g'(\theta))^2 + (g(\theta))^{-2} g''(\theta)\right) \quad (7)$$

Then

$$g(0) = V_l, \quad g'(0) = 0, \quad g''(0) = -2(V_l - V_r)$$

$$f(0) = 1, \quad f'(0) = 0, \quad f''(0) = -V_l(V_l^{-2}(-2(V_l - V_r))) = \frac{2(V_l - V_r)}{V_l}$$

So, the second order Taylor expansion of $f(\theta)$ at $\theta = 0$ is as follows:

$$f(\theta) = f(0) + \frac{1}{1!}f'(0)\theta + \frac{1}{2!}f''(0)\theta^2 + O(\theta^3)$$

$$= 1 + \frac{V_l - V_r}{V_l}\theta^2 + O(\theta^3) \quad (8)$$

$$\approx 1 + \frac{V_l - V_r}{V_l}\theta^2 \quad (9)$$

In Eq. (8), $O(\theta^3)$ is the remainder of the Taylor polynomial. For the coordinate system given in Fig. 1, we assume the angle $\theta > 0$ if θ is counter-clockwise from the radial direction. Otherwise, $\theta < 0$ if θ is clockwise from the radial direction. Eq. (9) shows that the ratio of $V(\theta)$ to V_r approximates a parabolic curve with the symmetric axis $\theta = 0$, and the second order coefficient $(V_l - V_r)/V_l \in (0, 1)$.

3. Materials and methods

Eight live trees located at the university arboretum in Zhejiang Agricultural and Forestry University were acoustically tested using a ARBOTOM tool (Rinntech, Heidelberg, Germany). The trees tested included Camphor (*Cinnamomum camphora*), Chinese maple (*Acer buergerianum*), abele (*Populus alba*), Chinese catalpa (*Catalpa ovata*) and Chinese red pine (*Pinus tabuliformis*). Fig. 2a shows the field setup of stress wave testing on a camphor tree.

The ARBOTOM unit consisted of twelve impulse sensors with cables, 60 mm sensor pins, and a 12 V rechargeable battery pack. Sensor No. 1 was first attached to the tree trunk through a sensor pin, a meter above the ground. Other eleven sensors were attached to the other side of the trunk and evenly spaced along a vertical

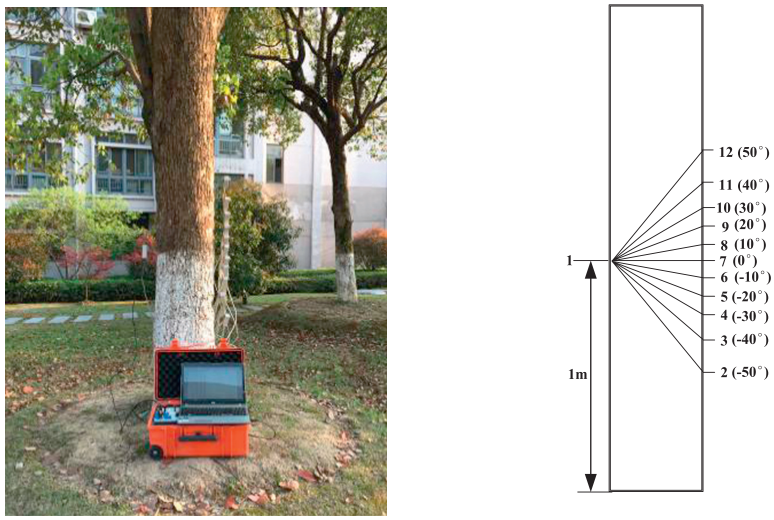

(a) The setup of field testing (b) The paths of stress wave measurements

Fig. 2. Longitudinal stress wave testing setup of live trees.

line (in *LR* plane). These eleven sensors were arranged in such a way that sensor No. 7 was placed directly opposite to sensor No. 1, and the angles difference between two neighbor propagation directions was 10°. Fig. 2b shows the sensor arrangement and the paths of stress wave measurements.

During testing, sensor No. 1 was used to introduce stress wave pulses into the trunk, and all other eleven sensors at the opposite side of the trunk received stress wave signals and the transmission times from sensor No. 1 to the receiving sensors were recorded by the system, then the software calculated the wave velocity along each path.

In order to compare the stress wave velocity patterns of sound wood with those of defective wood, we selected a 1.5 m long sound Chinese white poplar (*populus tomentosa*) log for laboratory testing (Fig. 3a). The sensors were attached in the log in a similar manner as live tree testing, but with 10 sensors and the propagation path angle θ ranged from 0° to 90° in *LR* plane, and the measured velocities were recorded. Then a 40 × 15 cm rectangle opening was cut through in the log (Fig. 3b). The longitudinal wave velocities for the "defective log" were measured while all the sensors were kept the same as in the sound log. Fig. 3 shows the testing setup for measuring stress wave velocities in the sound and defective log. From Fig. 3b, it can be seen that the stress wave with direction angle $50° \leqslant \theta < 90°$ passed through the cavity area.

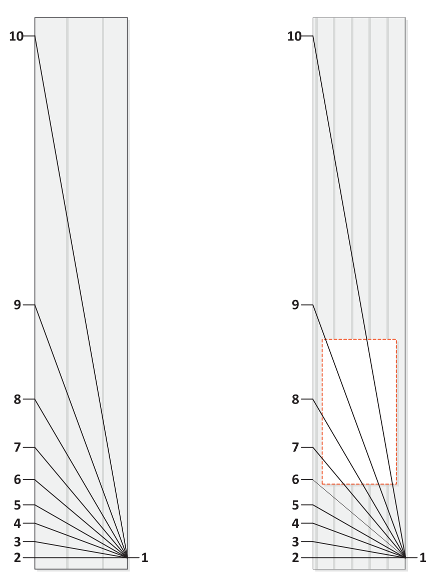

(a) Sound log (b) Log with cavity

Fig. 3. *LR* planes of sound log and defective log.

4. Results and discussion

4.1. Stress wave velocity pattern in LR plane of camphor trees

Four healthy camphor trees were tested, and the direction angle θ of the wave propagation path was from −50° to 50°. The measurements of stress wave velocity (m/s) of four sample trees are given in Table 1. Here, $V_i(\theta)$ represents the stress wave velocity along the path with direction angle θ for the *i*th sample tree ($i = 1, 2, 3, 4$).

For simplicity, we used radian as the unit of angle for regression analysis ($1° = \pi/180$ (radian)). Fig. 4 shows the regression curves of the wave velocity data sets presented in Table 1. It can be seen that for each sample tree, stress wave velocity increased with the direction angle θ, and the lowest velocity was always in radial direction ($\theta = 0$). Generally, each fitted curve approximated to a second order parabolic curve, which fitted to the theoretical model (9). The regression function between V_θ/V_0 and θ, and the coefficients of determination (R^2) are presented in Table 2.

In Table 2, the variable *y* represents the velocity ratio V_θ/V_0, and *x* represents the direction angle θ. The quadratic regression function of longitudinal stress wave velocity for each sample tree fitted the data very well with a coefficient of determination (R^2) above 0.92. It was also noted that the coefficient of the first degree term approximated to 0, and the constant term approximated to 1, indicating that the experimental results were in a good agreement with the theoretical model (9).

To study the stress wave velocity pattern in different species of trees, like the above-mentioned testing procedure, we measured the longitudinal stress wave velocities in the *LR* planes of other four live trees including Chinese maple, abele, Chinese catalpa, and Chinese red pine. We also found that the wave velocity

Table 1
Stress wave velocities measured in *LR* plane of healthy camphor trees (unit: m/s).

θ	−50°	−40°	−30°	−20°	−10°	0	10°	20°	30°	40°	50°
$V_1(\theta)$	1698.7	1524.6	1418.1	1334.8	1301.8	1301.4	1313.6	1346.7	1388.2	1436.3	1671.2
$V_2(\theta)$	1756.8	1632.6	1580.9	1468.6	1437.8	1441	1475.7	1506.4	1594.1	1690.2	1819.2
$V_3(\theta)$	1856.7	1586.6	1500	1484.3	1455	1328.9	1460.4	1434.3	1485.5	1711.5	1896.3
$V_4(\theta)$	1858.1	1685.4	1672.3	1609.6	1476.8	1437.5	1452.3	1581.9	1658.3	1821.9	1889.9

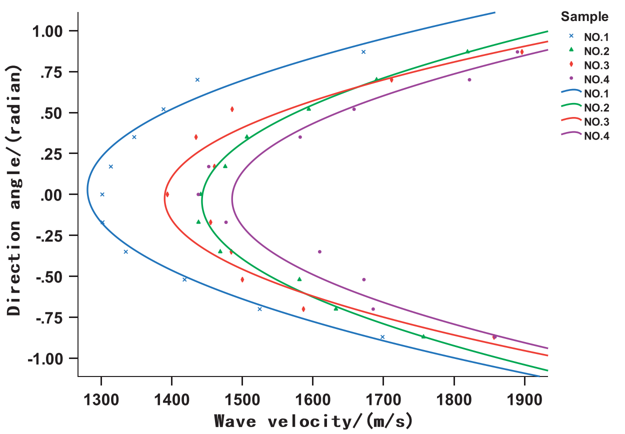

Fig. 4. Fitted curves of longitudinal stress wave velocities.

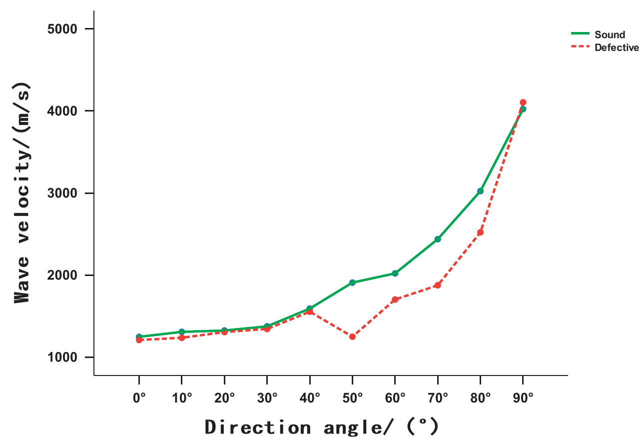

Fig. 6. Comparison of stress wave propagation velocities between sound and "defective" log.

Table 2
Quadratic regression model of V_θ/V_0 in healthy live trees.

Sample #	Regression function	R^2
1	$y = 0.3792x^2 - 0.0218x + 0.9842$	0.958
2	$y = 0.3173x^2 + 0.0252x + 1.0017$	0.989
3	$y = 0.4241x^2 + 0.021x + 0.9974$	0.922
4	$y = 0.3751x^2 + 0.0213x + 1.0336$	0.923

increased with the direction angle θ, and the lowest velocity was along the radial direction. Fig. 5 shows the testing fields and the fitted curves of stress wave velocities of all the sample trees. The regression functions of the wave velocities also approximated to the theoretical model (9) with the determination coefficient R^2 above 0.9 for each sample tree.

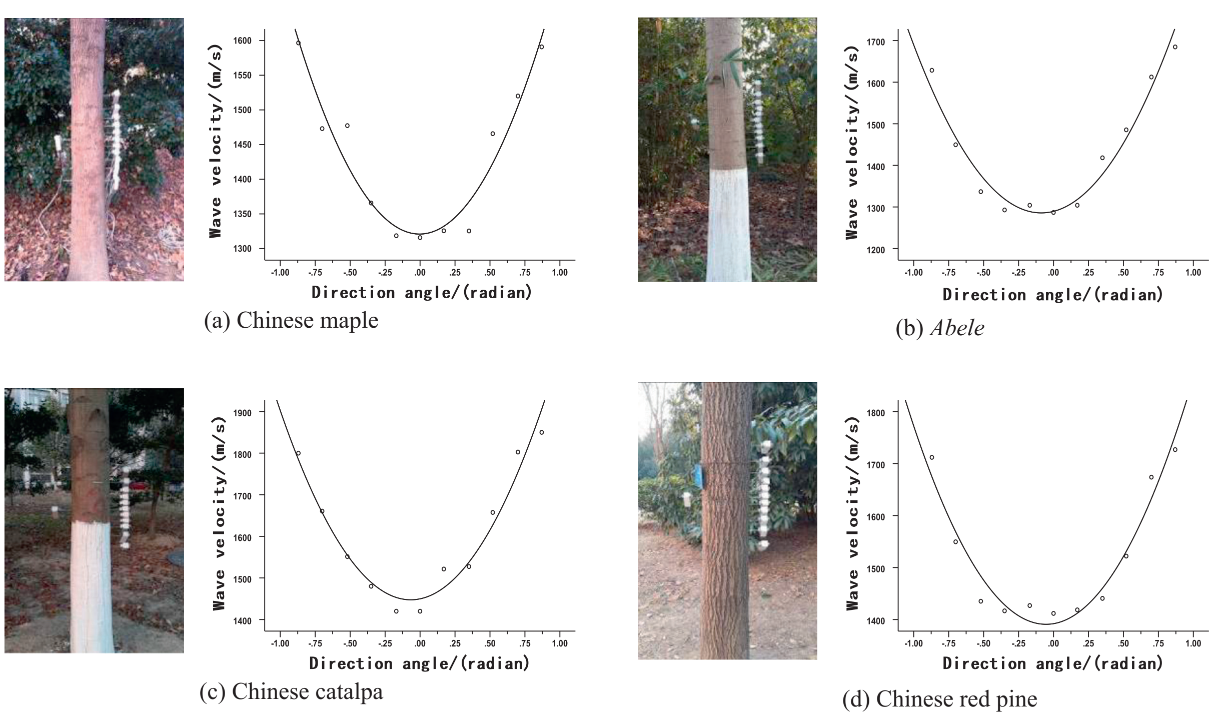

(a) Chinese maple

(b) *Abele*

(c) Chinese catalpa

(d) Chinese red pine

Fig. 5. Stress wave propagation velocity trend lines of different trees.

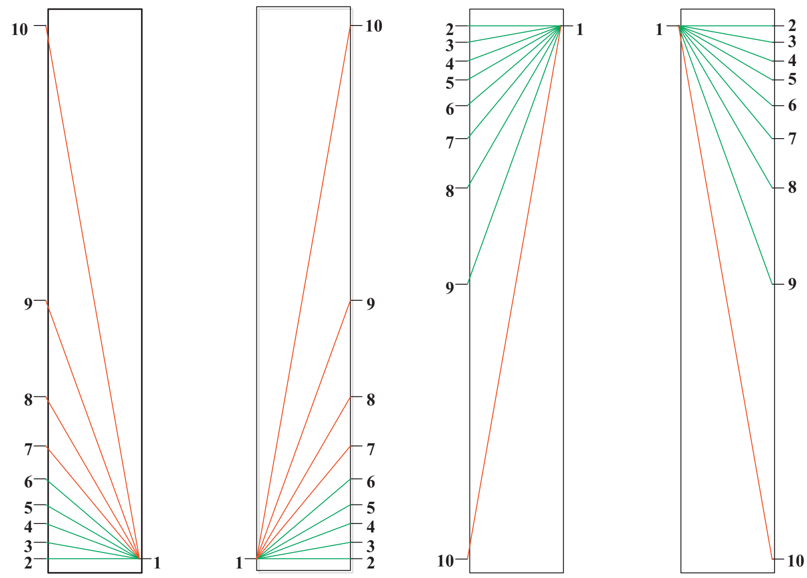

Fig. 7. Four-way-cross testing procedure.

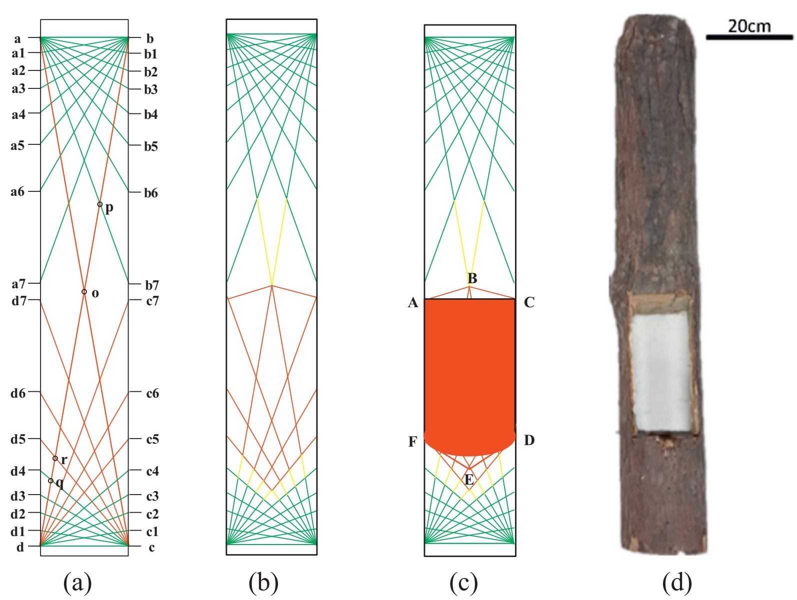

Fig. 8. Comparison between the diagnosed defect (red area) and actual cavity. (For interpretation of the references to colour in this figure legend, the reader is referred to the web version of this article.)

4.2. Comparison of the stress wave velocity patterns in LR plane between sound wood and defective wood

As shown in Fig. 3, a 1.5 m long sound poplar log was selected for laboratory testing, and then a 40 × 15 cm rectangle opening was cut through in the log. The measured velocities of both sound log and "defective" log were recorded. Fig. 6 shows the changing patterns of longitudinal stress wave velocities in the sound and defective log with respect to the wave propagation path (θ). The velocity-θ relationship for the sound log followed a second order parabolic curve as the case of healthy trees. The effect of the "cavity" in the log can be observed as the velocity-θ relationship (dash line) deviated from the smooth parabolic curve (solid line). The wave velocities measured at propagation paths (θ) of 50°, 60°, 70° and 80° in the "defective" log were significantly lowered than the velocities measured in the sound log. Consequently, the longitudinal velocity pattern in the "defective" log showed a deviation from the theoretical model (9).

4.3. Potential application of longitudinal wave velocity pattern in LR plane of wood

Current stress wave technology for decay detection on urban trees focuses on testing the cross section of a tree trunk. Information of wood property changes along the tree height is typically not considered. It is possible that the longitudinal velocity patterns along the tree height can be used to expand the coverage of stress wave testing, especially for constructing more accurate 3D acoustic tomographic images of a tree.

A four-way-cross testing procedure can be implemented in field tree inspection practice to improve the accuracy of diagnosis in a potential defective live tree. We first measure the wave velocities in the longitudinal direction ($\theta = 90°$) and radial direction ($\theta = 0°$) of sound wood. Second, derive the theoretical velocity model according to the formula (9). Third, measure stress wave velocities along different propagation paths over the trunk section under inspection. With the theoretical velocity model and actual measured velocities, the defect area can be detected and located. For instance, the "cavity" area given in Fig. 3(b) can be tested from four directions (started from the four vertexes of *LR* plane), and the measured velocities can be compared with those derived from the theoretical model, then all the defective lines can be decided. After comparison and cross-analysis of the velocities from different directions, the intersection of two defective lines designates the defect location, which is marked as a red area. Fig. 7 describes the four-way-cross testing procedure. Here, the red lines denote defective lines, and the green lines are the sound lines.

To evaluate the availability of the proposed four direction cross-testing procedure, we conducted another experiment. We chose a poplar log with the "cavity" shown in Fig. 8d, and its *LR* plane is given in Fig. 8a. From Fig. 8a–c, we can see the strategies to perform stress wave testing. Four test points *a*, *b*, *c* and *d* were selected to initiate stress impulses. The same testing procedures as that we experimented in live trees in this study were used to perform field stress wave testing, and the actual velocities from four different directions were measured with an ARBOTOM tool. Following testing, we calculated the theoretical velocities along all the directions with the theoretical velocity model, and compared the measured velocities with the theoretical velocities so that we can decide which path may be defective. In Fig. 8, the defective paths were marked by red color. After analyzing all the intersections of the defective lines, a hexagon ABCDEF was marked as the defective area. From Fig. 8c and d, it can be seen that the size and location of the detected defect area approximated the actual cavity area very well.

5. Conclusions

In this study, we proposed a theoretical model for the stress wave velocity patterns in the longitudinal–radial plane of a tree trunk. When a stress wave propagates in the *LR* plane along the tree trunk at a propagation path of angle θ (with respect to the radial direction), the ratio of the wave velocity to the radial velocity approximates a second-order parabolic curve. We conducted field stress wave testing on eight live trees of six species and laboratory testing on sound and defective logs. The measured velocities in healthy trees were found in a good agreement with the theoretical model. The results indicated that the stress wave velocity patterns can be used to diagnose internal defects in urban trees and improve the accuracy of 3D tomographic images in tree inspection applications.

Acknowledgements

This research was made possible by the collaboration between the USDA Forest Service, Forest Products Laboratory and Zhejiang Agriculture and Forestry University in China. This study was supported in part by the National Natural Science Foundation of China (Grant No. 61472368, 61302185, 61272313) and Zhejiang Provincial International Science and Technology Cooperation Project (Grant No. 2013C24026).

References

Berndt, H., Schniewind, A.P., Johnson, G.C., 1999. High-resolution ultrasonic imaging of wood. Wood Sci. Technol. 33, 185–198.

Bucur, V., 2003. Nondestructive Characterization and Imaging of Wood. Springer-Verlag, Berlin Heidelberg, Germany.

Dikrallah, A., Hakam, A., Kabouchi, B., Brancheriaum, L., Bailleres, H., Famiri, A., Ziani, M., 2006. Experimental analysis of acoustic anisotropy of green wood by using guided waves. ESWM-COST Action E35, 149–154.

Divos, F., Divos, P., 2005. Resolution of stress wave based acoustic tomography. In: Proceedings of the 14th International Symposium on Nondestructive Testing of Wood. University of Applied Sciences, Eberswalde, Germany, May 2–4, 2005.

Forest Products Laboratory, 2010. Wood handbook: wood as an engineering material. General Technical Report FPL-GTR-190, Madison, U.S. Department of Agriculture, Forest Service, Forest Products Laboratory, WI, p. 508.

Gerhards, C.C., 1982. Longitudinal stress waves for lumber stress grading—factors affecting applications: state of art. For. Prod. J. 32 (2), 20–25.

Guntekin, E., Emiroglu, Z.G., Yilmaz, T., 2013. Prediction of bending properties for Turkish red pine (*pinus brutia Ten.*) lumber using stress wave methods. Bioresources 8 (1), 231–237.

Hasegawa, Masumi, Yano, Yuji, Matsumura, Junji, Oda, Kazuyuki, 2012. Prospects for within-tree variation of the acoustoelastic behaviors in Japanese cedar. NDT&E Int. 49, 57–63.

Lawday, G., Hodeges, P.A., 2000. The analytical use of stress waves for the detection of decay in standing trees. Forestry 70 (5), 447–456.

Li, G., Wang, X., Feng, H., Wiedenbeck, J., Ross, R.J., 2014. Analysis of wave velocity patterns in black cherry trees and its effect on internal decay detection. Comput. Electron. Agric. 104, 32–39.

Liang, S., Fu, F., Lin, L., Hu, N., 2010. Various factors and propagation trends of stress waves in cross sections of Euphrates poplar. For. Prod. J. 60 (5), 440–446.

Lin, C., Kao, Y., Lin, T., Tsai, M., Wang, S., Lin, L., Wang, Y., Chan, M., 2008. Application of an ultrasonic tomographic technique for detecting defects in standing trees. Int. Biodeterior. Biodegr. 62 (4), 434–441.

Maurer, H.R., Schubert, S.I., Bachle, F., Clauss, S., Gsell, D., Dual, J., Niemz, P., 2005. Application of nonlinear acoustic tomography for nondestructive testing of trees. In: Proceedings of the 14th International Symposium on Nondestructive Testing of Wood. University of Applied Sciences, Eberswalde, Germany, pp. 339–349, May 2–4, 2005..

Najafi, S.K., Shalbafan, A., Ebrahimi, G., 2009. Internal decay assessment in standing beech trees using ultrasonic velocity measurement. Eur. J. For. Res. 128, 345–350.

Pellerin, R.F., Ross, R.J., 2002. Nondestructive Evaluation of Wood. Forest Products Society, Madison, WI, USA, p. 210.

Ross, R.J., Pellerin, R.F., 1994. Nondestructive testing for assessing wood members in structures—a review. General Technical Report FPL-GTR-70, Madison, U.S. Department of Agriculture, Forest Service, Forest Products Laboratory, WI, p. 40.

Socco, L.V., Sambuelli, L., Martinis, R., Comino, E., Nicolotti, G., 2004. Feasibility of ultrasonic tomography for nondestructive testing of decay on living trees. Res. Nondestr. Eval. 15, 31–54.

Wang, X., 2013. Acoustic measurements on trees and logs: a review and analysis. Wood Sci. Technol. 47 (5), 965–975.

Wang, X., Divos, F., Pilon, C., Brashaw, B.N., Ross, R.J., Pellerin, R.F., 2004. Assessment of decay in standing timber using stress wave timing nondestructive evaluation tools: a guide for use and interpretation. General Technical Report FPL-GTR-147, Madison, U.S. Department of Agriculture, Forest Service, Forest Products Laboratory, WI, p. 12.